Research article

A novel potential cause of extreme precipitation in the northwest China

Zhenming Ji [a,b,c,*], Shuting Tian [a]

[a] *School of Atmospheric Sciences, Sun Yat-sen University, Zhuhai, 519082, China*
[b] *Key Laboratory of Tropical Atmosphere-Ocean System, Ministry of Education, Zhuhai, 519082, China*
[c] *Southern Marine Science and Engineering Guangdong Laboratory (Zhuhai), 519082, China*

ARTICLE INFO

ABSTRACT

The northwest China is a climate change-sensitive and ecologically vulnerable area. Under the backdrop of global warming, this region exhibits clear characteristics of warming and wetting. In recent years, the causes of climate change in the northwest China has become a widely-focused topic. Previous research has mainly attributed the increase in precipitation to changes in the westerly belt and enhanced local convective activity caused by global warming. South Asia, beside the Tibetan Plateau from the northwest China, is one of the regions with the fastest growth in global atmospheric pollutant emissions. This study utilizes reanalysis data such as ERA5 and MERRA-2. Statistical methods, including Theil-Sen Median trend analysis and Singular Value Decomposition analysis, are employed to analyze the spatiotemporal characteristics of South Asian aerosols, extreme precipitation in the northwest China, and the correlation between the two. The study reveals the existence of two key aerosol-precipitation response areas. Synthetic analysis of the meteorological elements of the response events in both regions is conducted to explore the possible physical mechanisms behind the correlation between South Asian aerosols and precipitation in the northwest China. The result of this study is to provide a new perspective on the causes of extreme precipitation in the arid region of northwest China.

1. Introduction

Against the backdrop of global warming, regional climate change is occurring in various regions. China's northwest region (NWC), situated in the heartland of Eurasia, is one of the most vulnerable and ecologically fragile areas responding to climate change [1]. Shi et al. [2] proposed the hypothesis of "warm-humidification" in the NWC, noting the transition from warm and dry to warm and humid climate based on observations of temperature, precipitation, river runoff, and lake levels. Observations indicate that the increase in precipitation in the NWC is primarily driven by extreme precipitation events and intense convective rainfall [3]. Notably, the occurrence of extreme precipitation phenomena in the Taklamakan Desert has attracted attention. Despite being one of the driest regions in China with minimal annual precipitation, it experiences sporadic but intense rainfall events, posing risks to the region's low vegetation coverage and loose soil [4].

The causes of these changes in the NWC's precipitation are not fully understood but can be categorized as follows:

a. Strengthening of the westerly circulation and upward motion: The westerly belt's moisture transport and the intensified westerly circulation contribute to increased precipitation in the NWC [5]. The strengthening of upward motion may be related to the weakened compensatory sinking airflow around the Tibetan Plateau caused by increased precipitation in surrounding areas [6,7].
b. Changes in moisture transport in the eastern NWC: The increasing trend in integrated water vapor flux in the NWC is attributed to reduced output water vapor flux at the eastern boundary rather than increased input from other directions [8]. The weakening of the East Asian summer monsoon and the westward extension of the western Pacific subtropical high facilitate moisture transport from the Indian Ocean and the Pacific Ocean, resulting in amplified input water vapor flux in the eastern NWC and increased precipitation [9].
c. Increased moisture transport associated with the Indian summer monsoon: Studies suggest that the northward transport of moisture from the Arabian Sea significantly influences precipitation variations in the Tarim Basin [10]. Anomalous pressure gradient forces caused by potential height field variations over Central Asia and the Arabian Sea lead to excess summer precipitation in southern Xinjiang. Moisture from the Indian Ocean, driven by stronger meridional circulation, plays a crucial role in heavy rainfall formation in northern Xinjiang [11].

South Asia is located on the southern slope of the Tibetan Plateau, where black carbon and dust aerosols absorb shortwave radiation, leading to atmospheric heating. This creates an elevated heat pump effect [12–14], causing warm air to ascend and bringing in warm and moist air to South Asia. The effect also shifts the convective instability zone northward, leading to deep convection over the Himalayas and the southern Tibetan Plateau [15]. These findings are based on experiments using Global Climate Models (GCMs), which have been supported by using the Community Climate Model version 3 (CCM3) [16] and Community Atmosphere Model version 3 (CAM3) models [17]. They confirm the significant impact of black carbon and dust aerosols on local circulation in South Asia. Reanalysis data and numerical simulations have further confirmed the existence of the elevated heat pump effect and researchers have explored its associated atmospheric dynamics and thermodynamic mechanisms. Wang et al. [17] used the CAM3 model to analyze how South Asian aerosols affect the summer monsoon. Black carbon aerosols heat the lower atmosphere, causing an earlier onset of the monsoon. The heated atmosphere ascends along the Tibetan Plateau, creating a warm anomaly center and strengthening the monsoon due to the temperature gradient with the South Asian continent. Additionally, numerous studies have indicated that aerosols have an impact on the South Asian monsoon [18–20], and even on the Asian monsoon as a whole [21].

In the northwest region, isolated rainfall events influenced by the South Asian summer monsoon occasionally occur, despite its limited reach. Du et al. [22] used the Weather Research and Forecasting (WRF) model and isotope tracing to analyze intense precipitation events in the arid northwest region. Isotope tracing confirmed that monsoonal moisture, sourced from the ocean, is responsible for long-distance moisture transport and subsequent rainfall. WRF simulations further supported the attribution of these precipitation events to the summer monsoon, rather than local convection.

In summary, the elevated heat pump effect caused by South Asian aerosols triggers an early and intensified onset of the South Asian summer monsoon, leading to increased moisture influx into the northwest region. This suggests that the amplified South Asian summer monsoon, driven by the aerosol-induced elevated heat pump effect, could potentially result in heightened precipitation in the NWC.

Does South Asia aerosols have potential impact on the warm-humidification in the NWC? This study aims to examine the connection between South Asian aerosols and precipitation variations. It seeks to explore the potential influence of South Asian aerosols on the intensity of moisture transport from South Asia to the northwest region by modifying atmospheric circulation. This, in turn, may alter the temporal characteristics of extreme precipitation events in the NWC.

Aerosols have weaker climate effects compared to other factors (e.g. greenhouse gases, internal variability within the climate system). Identifying and separating their impact on climate is challenging when analyzing aerosol optical parameters and meteorological variables. However, aerosols have a significant influence on extreme precipitation events [23], which show a more important potential impact on the NWC [24]. Thus, this study focuses on the impact of South Asian aerosols on extreme precipitation events rather than mean precipitation.

2. Datasets and methods

The study area (Fig. S1) encompasses the region between approximately 31°N to 50°N latitude and 73°E to 111°E longitude, constituting approximately 30 % of China's land area. This region typically includes Ningxia Hui Autonomous Region, Xinjiang Uygur Autonomous Region, Qinghai, Shaanxi, and Gansu provinces. It is encircled by majestic mountain ranges, such as the Altai Mountains in the northwest, Kunlun Mountains in the southwest, Qilian Mountains in the east, and Helan Mountains in the northeast. Consequently, these mountains impede the movement of moist air masses carried by the atmospheric circulation, resulting in a pronounced rain shadow effect and the formation of expansive desert basins, including the Tarim Basin, Junggar Basin, and Qaidam Basin. The northwest region exhibits a typical continental climate, with an average annual temperature of around 8 °C. Temperature variations across the area are significant, and the average annual precipitation is below 200 mm. In comparison to the humid regions of southeastern China, the northwest region is predominantly arid and experiences less influence from the Asian monsoon.

2.1. Datasets

The daily precipitation data used in this study is derived from the CN05.1 dataset, which covers mainland China from 1980 to 2020. This dataset has been carefully curated by the National Meteorological Information Center of China and is based on high-quality precipitation measurements collected at around 2400 national weather stations. The CN05.1 dataset employs advanced

interpolation techniques, including anomaly approximation, to generate gridded precipitation data with a horizontal resolution of $0.25° \times 0.25°$ [25].

The AOD (Aerosol Optical Depth) data used in this study is obtained from the (Modern-Era Retrospective analysis for Research and Applications, version 2) MERRA-2 dataset. This dataset incorporates ground-based AErosol RObotic NETwork (AERONET) observations and satellite remote sensing AOD data from Advanced Very High Resolution Radiometer (AVHRR), Multi-angle Imaging Spectroradiometer (MISA), and Moderate Resolution Imaging Spectroradiometer (MODIS), assimilated using the Goddard Earth Observing System Model, Version 5 (GEOS-5) model. The MERRA-2 dataset provides various atmospheric parameters, including water vapor, temperature, precipitation, radiation, and aerosols, since 1980. With the Goddard Chemistry Aerosol Radiation and Transport (GOCART) module integration, GEOS-5 simulates optical properties and mixing ratios of five aerosol types (black carbon, dust, sulfate, sea salt, and organic carbon) [26]. The dataset has a spatial resolution of $0.5° \times 0.625°$ and can be downloaded from NASA's Goddard Earth Sciences Data and Information Services Center (GES DISC). This study utilized two sets of MERRA-2 data with different temporal resolutions. For the analysis of spatiotemporal variations in AOD over South Asia, monthly total AOD data at a wavelength of 550 nm from January 1980 to December 2020 were employed. For individual case analyses, AOD data at 550 nm wavelength with a temporal resolution of 3 h were used, along with data on black carbon, dust, sulfate, sea salt, and organic carbon AOD.

The ERA5 dataset is the fifth-generation global atmospheric reanalysis data released by the European Centre for Medium-Range Weather Forecasts (ECMWF). It offers higher spatiotemporal resolution compared to its predecessor, ERA-Interim. ERA5 provides a horizontal resolution of $0.25° \times 0.25°$ and increases the temporal resolution from 6 h to 1 h. With 137 vertical levels, it includes 240 variables covering temperature, radiation, precipitation, and more. Utilizing advanced data assimilation and modeling systems, ERA5 combines historical observations and satellite remote sensing data to produce more accurate atmospheric simulations. This study utilizes monthly ERA5 data from 1980 to 2020, focusing on variables such as temperature, wind components, humidity, cloud properties, geopotential height, and radiative fluxes. For case studies, daily mean values are computed based on the 00:00, 06:00, 12:00, and 18:00 UTC data for the selected variables.

2.2. Methods

The study employed the following statistical methods:

Pearson's correlation coefficient: Used the method developed by the British statistician Karl Pearson to calculate the correlation coefficient using the method of moments.

Theil-Sen Median Trend Analysis: Utilized the Theil-Sen Median method to simulate the trend and characterize the spatial pattern evolution of each grid point over a certain time series period. This method is effective in capturing the long-term evolution of AOD time series.

Mann-Kendall test: Applied a non-parametric statistical test, known as the Mann-Kendall test, to assess the long-term trends in meteorological variables such as temperature, precipitation, and air pressure. This method is suitable for trend analysis of non-normally distributed variables.

Singular Value Decomposition (SVD) analysis: Conducted SVD analysis on the cross-covariance matrix of two datasets with the same length in time but potentially different spatial domains. SVD analysis helps to separate coupled spatial modes that exhibit linear relationships with each other. It is a generalized approach to Empirical Orthogonal Function (EOF) analysis, aiming to explain the covariance between two variables rather than maximizing variance within a single variable.

The study employed the following extreme precipitation index calculation methods:

The Expert Team on Climate Change Detection and Indices (ETCCDI), established by organizations like the World Meteorological Organization (WMO) Climate Committee, has defined 27 typical climate indices, including 16 temperature indices and 11 precipitation indices. These indices effectively define extreme climate events and are widely applied in studies on extreme high temperatures and extreme precipitation [6,27]. Among the 11 precipitation indices, the following six commonly used extreme precipitation indices were selected for analysis (Table 1).

The calculation of regional extreme precipitation events is divided into two parts: extreme precipitation events (EP) and regional extreme precipitation events (REPE). Extreme precipitation events (EP) are defined as precipitation exceeding the 95th percentile of daily precipitation greater than 0.1 mm over a specified period of time. Regional extreme precipitation events (REPE) are determined by analyzing the number of grid points/stations within the study area that experience EP events on a daily basis. A time series of the number of grid points/stations is used to establish a 95th percentile threshold using the percentile method. Events surpassing this

Table 1
Extreme precipitation index, reference period is 1961–1990.

| Abbreviations	Full name	definition	units
RX1day	Maximum 1-day precipitation	The maximum daily precipitation in a year	mm
R10	Number of moderate wet days	The number of days in a year with precipitation exceeding 10 mm	day
R95PTOT	Total precipitation from very wet days	The cumulative annual precipitation from days with precipitation exceeding the 95th percentile value	mm
R99PTOT	Total precipitation from extremely wet days	The cumulative annual precipitation from days with precipitation exceeding the 99th percentile value	mm
PRCPTOT	Annual total precipitation	The total precipitation in a year from days with precipitation exceeding 1 mm	mm
CDD	Maximum length of dry spell	The longest consecutive period in a year with daily precipitation below 1 mm	day

threshold are considered as REPE [28].

3. Result

3.1. Variation and correlation between aerosols in the South Asia and extreme precipitation in the NWC

Fig. 1 shows the spatial distribution of seasonal AOD trends in South Asia from 1980 to 2020. Consistent patterns are observed across seasons, with notable differences between the northern and southern Himalayan regions. Increased AOD is prominent in the southern foothills, Indo-Gangetic Plain (IGP), and Ganges Delta, while the northern Himalayas, with fewer pollution sources, exhibit non-significant trends in spring and decreasing trends in other seasons. The heavily polluted South Asian subcontinent experiences rising aerosol concentrations due to increased emissions from fuel combustion, industry, and urban sources.

From 1980 to 2020, South Asia (6.5°N-40°N, 66.5°E−100°E) experienced significant fluctuations and upward trends in AOD across all seasons (Fig. S2), with clear interannual variations. The trends were as follows: 0.68/10 years for spring, 0.29/10 years for summer, 0.46/10 years for autumn, and 0.6/10 years for winter, with the highest increase observed in spring. This rise can be attributed to crop residue burning and forest fires on the southern slopes of the Himalayas during the pre-monsoon period. Peaks in AOD occurred in 1982 and 1991, likely due to volcanic eruptions of El Chichón and Pinatubo, releasing volcanic ash aerosols and causing abnormally high AOD values (Fig. S2). The sliding average curve of seasonal AOD shows a rapid increase from around 1995 to 2005, followed by a sustained higher level. After 2000, AOD fluctuations decreased, indicating a more stable trend, with spring and summer AOD declining after 2010, while autumn and winter AOD continued to rise.

Fig. 2 depicts the spatial distribution of trends in extreme precipitation indices in the NWC. The index representing total precipitation during very wet days (R95PTOT) shows an increasing trend in most areas. The range of R95PTOT trend rates is approximately
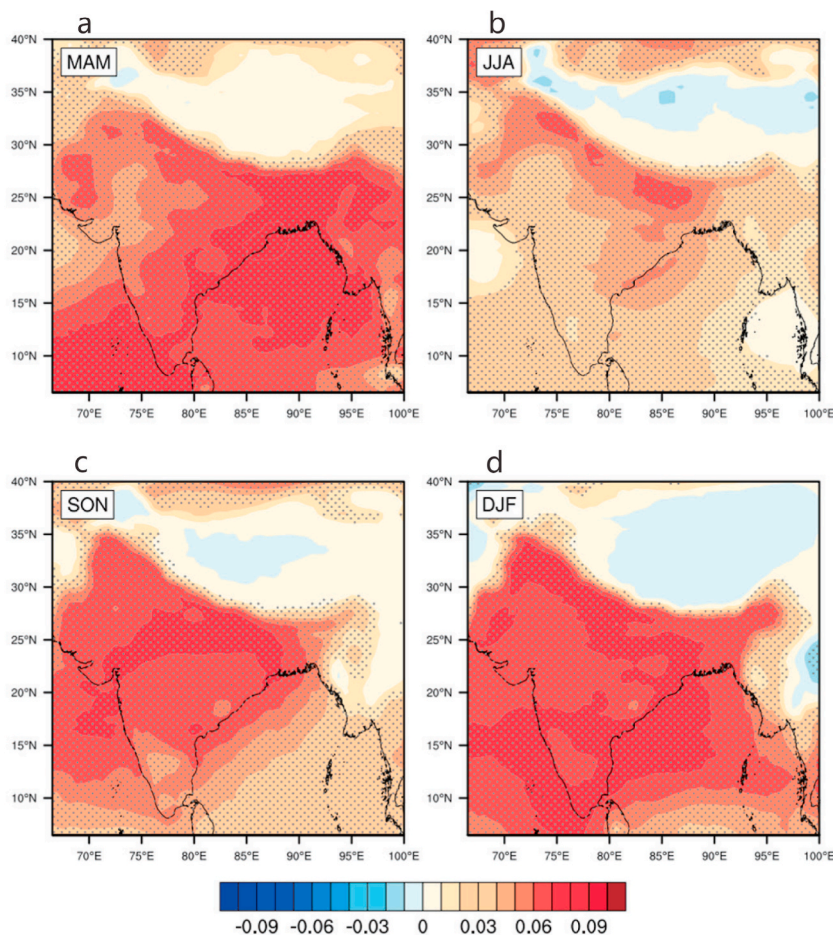
Fig. 1. The spatial distribution of standardized AOD trends in the South Asia during the four seasons (a. March-April-May, b. June-July-August, c. September-October-November, and d. December-January-February) from 1980 to 2020. The trends are represented by color shading (unit: year^{-1}), and areas marked with dots indicate statistically significant trends at a 90 % confidence level. (For interpretation of the references to color in this figure legend, the reader is referred to the Web version of this article.)

−1 to 2.5 mm/year. The increasing trend in R95PTOT is statistically significant (at the 90 % confidence level) in the northeastern regions of Xinjiang and Qinghai provinces. The trend distribution of the index representing total precipitation during extremely wet days (R99PTOT) is similar to that of R95PTOT, but with a smaller range of trend rates, approximately −0.5 to 1 mm/year. The regions with statistically significant increasing trends (at the 90 % confidence level) are mainly concentrated in northern Xinjiang and the northeastern region of Qinghai province. The trend range of the index representing the maximum 1-day precipitation amount (RX1day) is relatively small, approximately −0.1 to 0.1 mm/year. The trend in the index representing consecutive dry days (CDD) shows the opposite pattern compared to other extreme precipitation indices. Except for the Taklamakan Desert in the southern part of Xinjiang, most regions exhibit a decreasing trend in CDD, with a range of approximately −1 to 1 day/year. The index representing the number of heavy precipitation days (R10) shows the largest increasing trend in the Tianshan Mountains and the northeastern part of Qinghai province, with a trend rate of 0.1 day/year.

The extreme precipitation indices in the NWC display notable variability over both interannual and decadal scales. Except for CDD, all indices exhibit an upward trend, indicating a general rise in extreme precipitation (Fig. 3). The declining trend in CDD, representing consecutive dry days, mirrors the overall increase in extreme precipitation observed across the region, consistent with other indices.

For instance, R95PTOT ranges from 62 to 124 mm between 1980 and 2020, with a ten-year trend of 2.9 mm/10 years. Initially decreasing during the 1980s and 1990s, R95PTOT later shows an upward trend. Similarly, R99PTOT ranges from 16 to 43 mm, with a
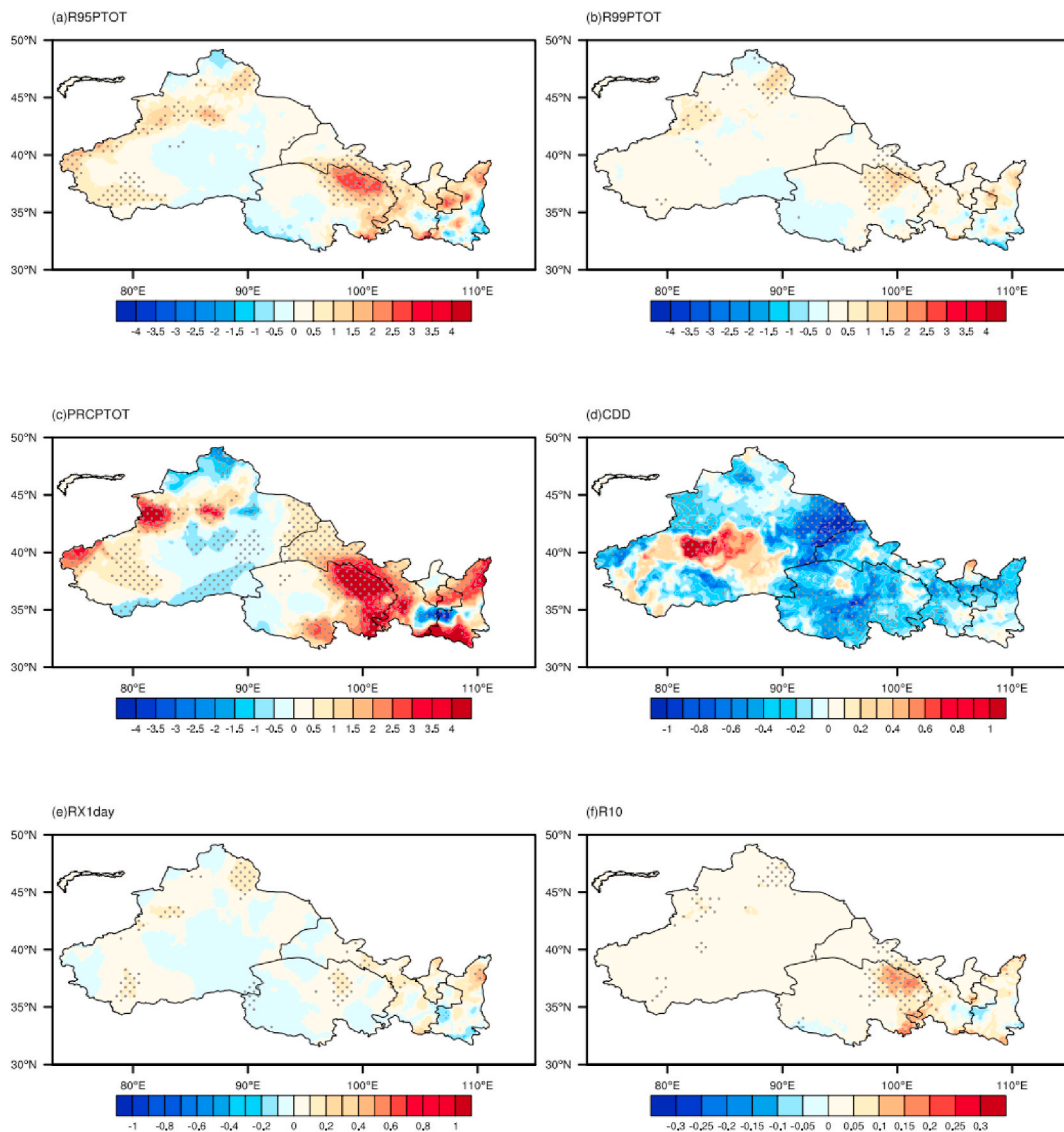
Fig. 2. The spatial distribution of trends in extreme precipitation indices from 1980 to 2020. Panels a–f show the trends for R95PTOT (mm/year), R99PTOT (mm/year), PRCPTOT (mm/year), CDD (day/year), RX1day (mm/year), and R10 (day/year), respectively. The color shading represents the trend values, and the areas with dots indicate statistically significant trends at the 90 % confidence level. (For interpretation of the references to color in this figure legend, the reader is referred to the Web version of this article.)
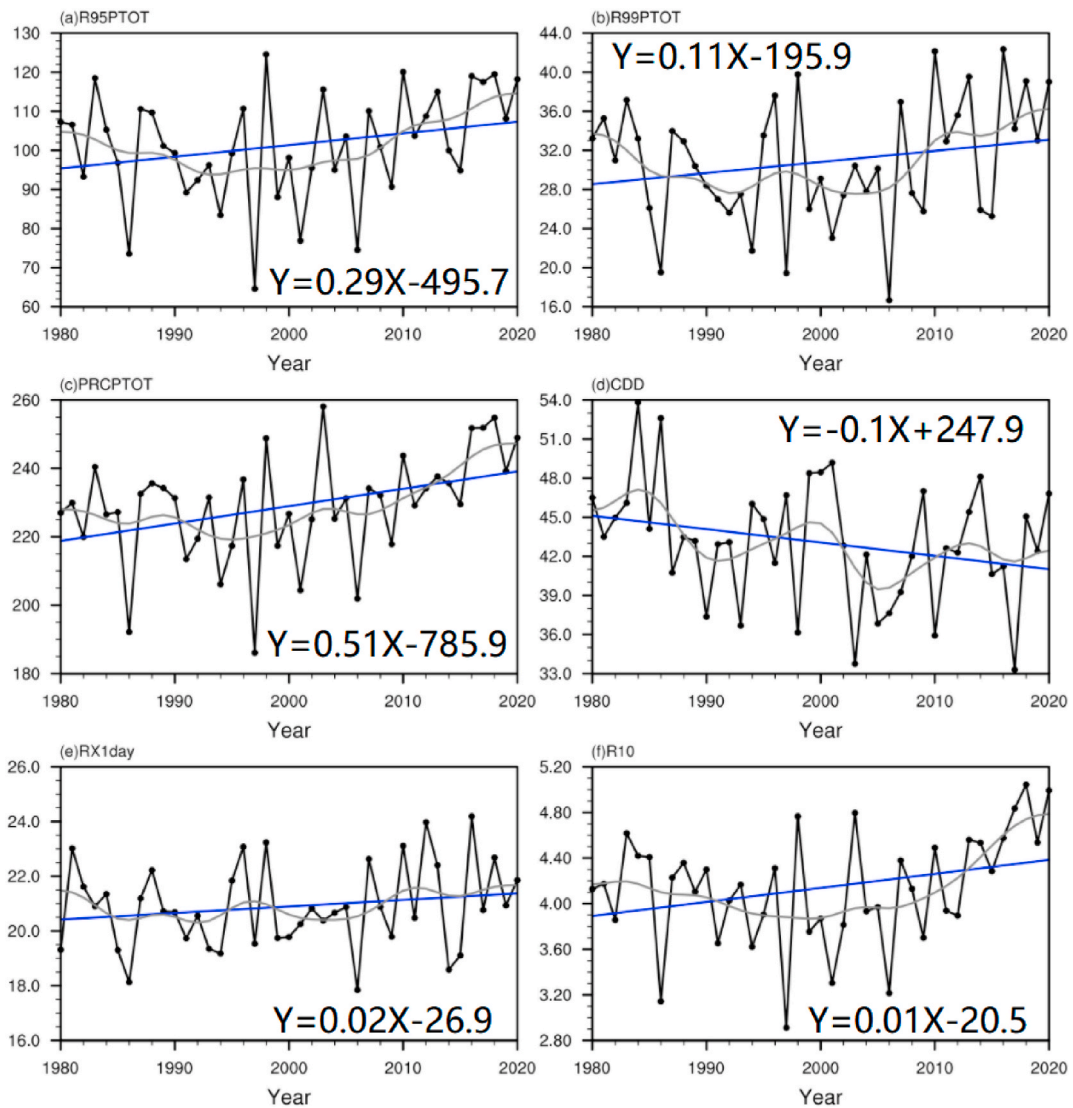
Fig. 3. The time series of extreme precipitation indices in the NWC from 1980 to 2020. The indices include (a) R95PTOT (mm), (b) R99PTOT (mm), (c) PRCPTOT (mm), (d) CDD (days), (e) RX1day (mm), and (f) R10 (days). The black solid line represents the original time series, the blue solid line represents the linear trend, and the gray solid line represents the 12-year moving average. (For interpretation of the references to color in this figure legend, the reader is referred to the Web version of this article.)

ten-year trend of 1.1 mm/10 years. This index exhibits more fluctuations, with peaks in 1990 and 2010 and troughs in 2004 and 2014.

PRCPTOT, ranging from 184 to 260 mm, displays a rapid increase from the mid-1990s to 2020, with a ten-year trend of 5.1 mm/10 years. RX1day remains relatively stable around 20 mm, with no significant trend observed, showing quasi-periodicity of 10 years.

Conversely, CDD varies from 33 to 54 mm, with a ten-year trend of −1 day/10 years, showing significant fluctuations with a quasi-periodicity of 14 years. R10 ranges from 2.8 to 5.2 days, with a ten-year trend of 0.1 day/10 years, initially decreasing until 2000, followed by an upward trend. Overall, extreme precipitation in the NWC has increased over time, with varying trends across different indices.

The increasing trends in AOD across South Asia and extreme precipitation indices in the NWC reflect the impact of human activities and global warming. Given the spatial variations in trends, it's essential to separately address local trends for each variable rather than considering a regional trend. Fig. 4 illustrates the spatial correlation between annual average AOD in South Asia and extreme precipitation indices in the NWC. Positive correlations between AOD and R95PTOT are observed mainly in the northern Tianshan Mountains in Xinjiang, southwestern Tarim Basin, Qinghai, northern Gansu, and Shaanxi, with a maximum coefficient of 0.3, indicating a weak positive correlation. Similar correlations are seen with R99PTOT, passing the 90 % significance test in specific regions.

Similarly, PRCPTOT exhibits correlations akin to R95PTOT and R99PTOT, except for a weak negative correlation in the northern Tianshan Mountains. The spatial correlation with RX1day is stronger, particularly in southern Xinjiang, northern Gansu, and southern
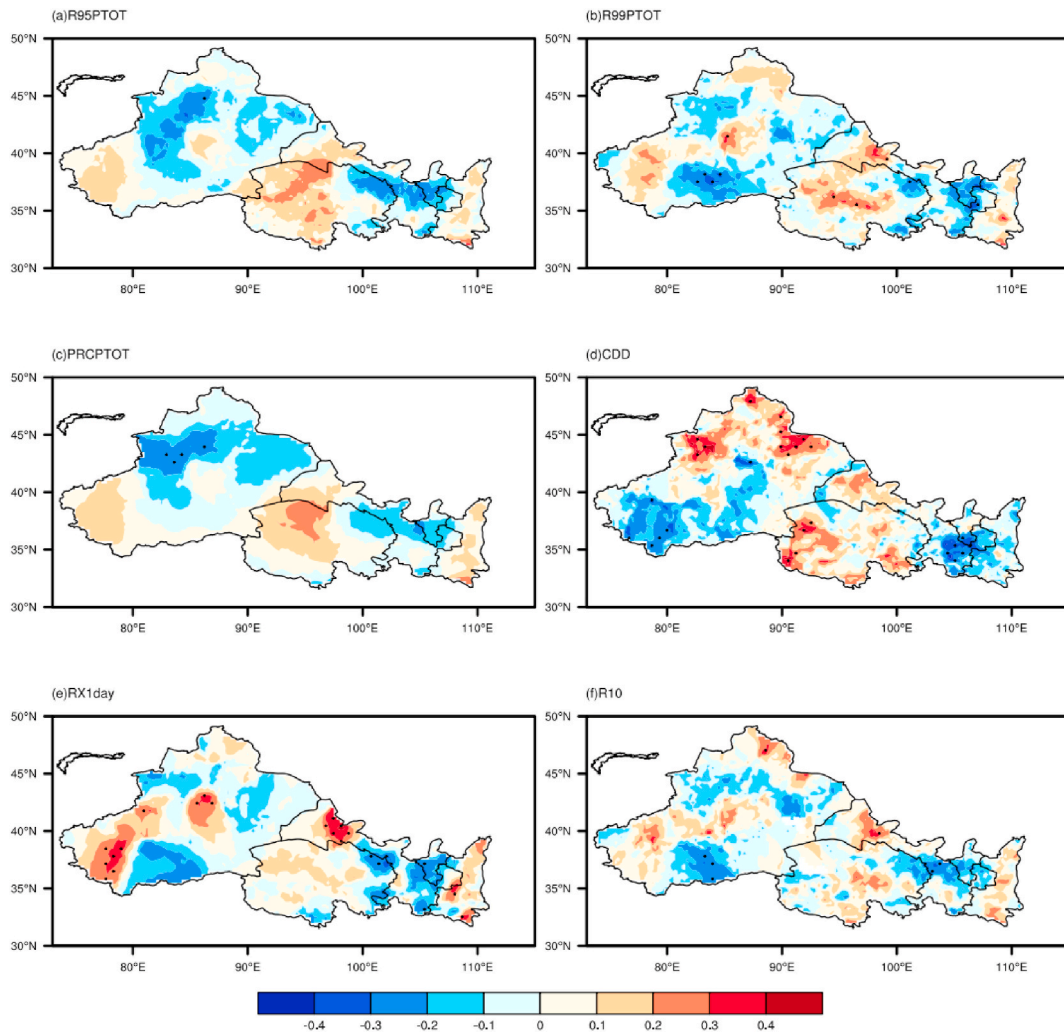
Fig. 4. The spatial distribution of the correlation between the annual average AOD in South Asia and the extreme precipitation indices (a. R95PTOT, b. R99PTOT, c. PRCPTOT, d. CDD, e. RX1day, f. R10) in NWC from 1980 to 2020. The figure uses color shading to represent the magnitude of the correlation coefficient, and marked regions with dots indicate significance at a 90 % confidence level. (For interpretation of the references to color in this figure legend, the reader is referred to the Web version of this article.)
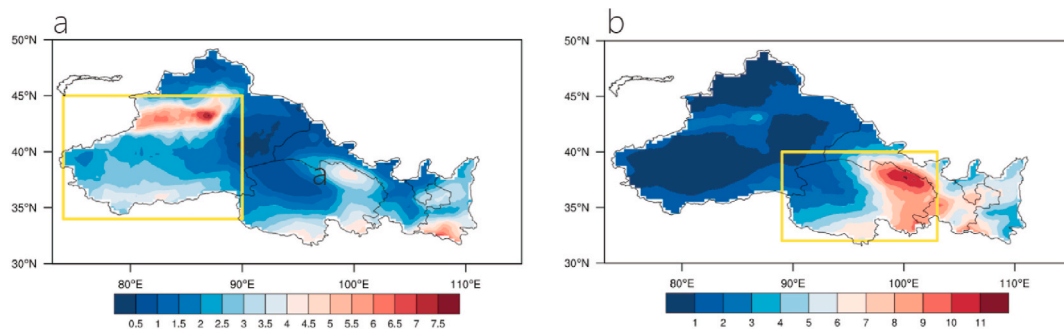
Fig. 5. Daily average precipitation (mm/day) synthesized from extreme precipitation events during the summer season from 1980 to 2020 in South Xinjiang (a) and Qinghai (b) regions, respectively. The yellow box in Fig. 5a represents the Key Response Zone I and the same one in Fig. 5b represents the Zone II. (For interpretation of the references to color in this figure legend, the reader is referred to the Web version of this article.)

Shaanxi, with coefficients surpassing 0.4 and passing significance tests.

Conversely, CDD, representing consecutive dry days, shows an opposite pattern, particularly in Qinghai and northern Gansu, suggesting that high aerosol levels in South Asia may lead to extreme precipitation in these areas, offsetting each other's effects and resulting in a relatively low correlation with total annual precipitation.

A correlation exists between AOD in South Asia and extreme precipitation in the NWC. To comprehensively understand this relationship, we delineate significant correlation regions into two key response areas: South Xinjiang (34°-45°N, 74°-90°E) and Qinghai (32°-40°N, 89°-103°E), denoted as Key Response Area I and Key Response Area II, respectively (see Fig. 5, yellow box).

Over the period from 1980 to 2020, Key Response Area I experienced 133 regional extreme precipitation events, while Key Response Area II had 154 such events. These events yielded average daily precipitation exceeding 11 mm/day, with South Xinjiang seeing concentrations primarily in the Tianshan Mountains and the southern Tarim Basin, and Qinghai focusing on the eastern Qaidam Basin and the Qilian Mountains (Fig. 5).

To address the lagged effect of South Asian aerosols on NWC precipitation, we define a three-day unit encompassing the day of an extreme event in South Xinjiang and the preceding two days. Analyzing 399 and 462 days, respectively, we calculate anomalies in South Asian aerosol levels compared to the average AOD during the summer season from 1980 to 2020. Notably, the AOD in South Asia corresponding to precipitation in South Xinjiang consistently exhibits high values, mainly concentrated in the Bay of Bengal and the Thar Desert in northwest India. Similarly, AOD anomalies corresponding to precipitation in Qinghai are also high, with concentrations in the central Bay of Bengal and Thar Desert, alongside elevated values in the Tibetan Plateau.

3.2. Analysis of South Asia aerosol and extreme precipitation response events in the NWC

We have chosen representative cross-regional aerosol-precipitation response events from the two key areas and utilized a synthesis analysis approach to investigate the atmospheric circulation characteristics linked to these events. This preliminary study aims to unveil the physical mechanisms by which South Asia aerosols impact extreme precipitation in the NWC.

#### 3.2.1. Case study in the Key Response Zone I

Fig. 6a presents a strong precipitation event that occurred on August 17, 2016, in regions such as Xinjiang and Gansu. The center of intense rainfall was situated in the Tianshan mountain range, the southern edge of the Taklimakan Desert, and the Mazongshan Gobi and Qilian Mountains in the northern part of Gansu Province, with daily precipitation exceeding 30 mm/day. Simultaneously, the area of intense precipitation corresponded well with the high-value regions of positive correlation between South Asia aerosols and extreme precipitation in South Xinjiang. This region is characterized by a temperate continental arid and semi-arid climate, with limited rainfall, and some areas experience an annual average precipitation of less than 50 mm. To gain a clearer understanding of the precipitation amount during this strong rainfall event, we selected the period from 1980 to 2010 as the baseline and calculated the 90th percentile threshold of climatological precipitation (Fig. 6b). The calculation involved sorting the precipitation amounts greater than 0.1 mm in ascending order from 1980 to 2010 and determining the 90th percentile as the precipitation threshold. It can be observed that the 90th percentile precipitation threshold in the NWC ranges from 0 to 15 mm, with noticeable spatial variations. The threshold decreases from south to north and from east to west. In the Tianshan mountain range region with higher precipitation, the 90th percentile threshold is around 7–9 mm. In the drier interior of southern Xinjiang, the threshold is around 3–5 mm. In the relatively humid southern Shaanxi region, the threshold is around 13–15 mm. By comparing Fig. 6a and Fig. b, it can be seen that the precipitation amount during this strong rainfall event exceeded the 90th percentile of climatological daily precipitation. In some areas, the precipitation amount during this event surpassed 50 % of the annual precipitation for that particular region.

During the above extreme precipitation event in South Xinjiang, the aerosol content in South Asia was also at a high level. Fig. 7a shows the percentage departure of the average AOD in South Asia from August 14th to 17th, 2016, compared to the climatological average AOD from August 14th to 17th, 1980–2020. The departure percentage is calculated by taking the difference between the AOD in 2016 and the climatological average AOD for the same period, dividing it by the climatological average AOD, and multiplying by
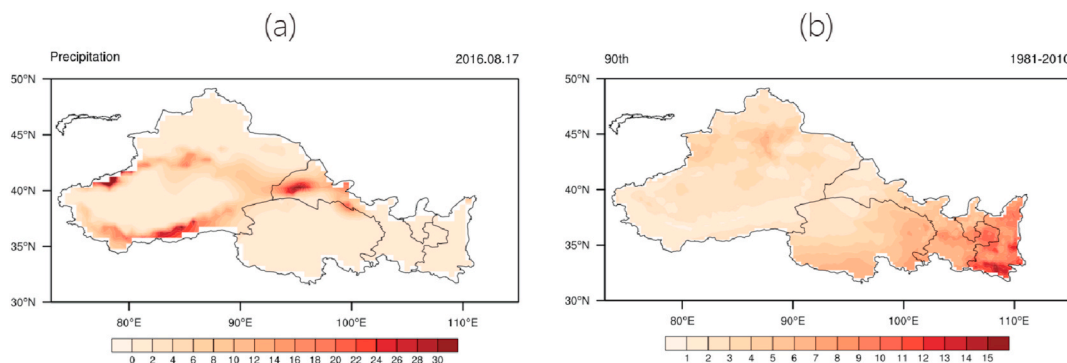
Fig. 6. The spatial distribution of precipitation in the NWC on August 17, 2016 (a) (unit: mm/day). The right panel shows the spatial distribution of the 90th percentile threshold of precipitation for the period 1981–2010 in the NWC (b) (unit: mm/day).
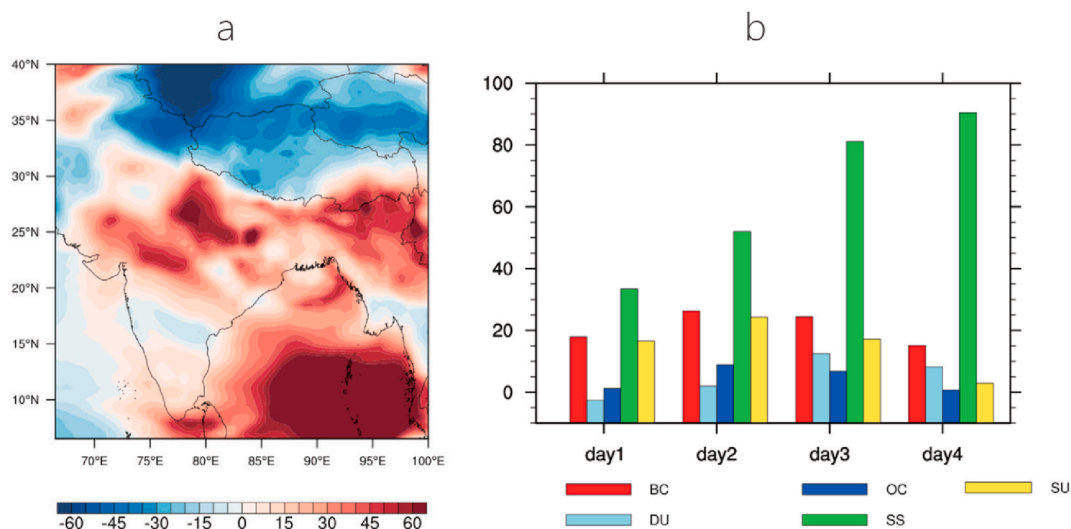
Fig. 7. The percentage departure of the average AOD in South Asia from August 14th to 17th, 2016, compared to the climatological average AOD from August 14th to 17th, 1980–2020 (a) (unit: %). The departure percentages of Black Carbon (BC), Dust (DU), Organic Carbon (OC), Sea Salt (SS), and Sulfate (SU) AOD in South Asia from August 14th to 17th, 2016, relative to the climatological mean (b) (unit: %).

100 %. The departure percentage reflects the deviation of AOD from the climatological mean during a pollution event. The image indicates that South Asia as a whole experienced high emission, suggesting a pollution event in the region. There is a center of abnormally high values in the Indo-Gangetic Plain, with AOD values more than 60 % higher than the 1980–2020 average.

To further understand the composition of aerosols in South Asia during this response event, the regional averages of Black Carbon (BC), Dust, Organic Carbon (OC), Sea Salt, and Sulfate AOD for August 14th to 17th, 2016, were calculated. The departure percentages of these aerosol components from the climatological mean were also calculated. Fig. 7b shows the results. Except for a small negative anomaly in dust aerosols on day 1, all other aerosol components showed positive anomalies during this response event. Sea salt aerosols exhibited a significant positive anomaly, which could be related to the abnormally high AOD values in the Bay of Bengal region. Additionally, black carbon and organic carbon aerosols showed higher emissions compared to the climatological mean.

The temperature profiles are shown in Fig. S3, with a meridional average taken from 85°E to 92°E, corresponding to the southern edge of the Tibetan Plateau and the longitude range associated with the center of high AOD anomalies. The difference field (Fig. S3c) clearly illustrates a temperature anomaly center in the near-surface, adjacent to the southern side of the Himalayas, with temperatures around 3 °C greater than the climatological state. This anomaly is likely related to the abundant presence of absorbing aerosols in the
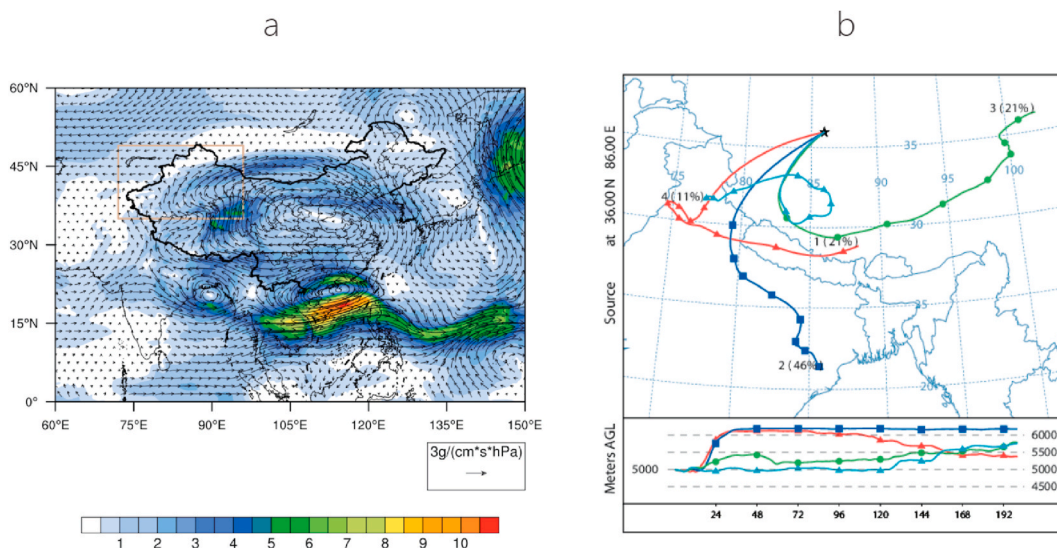
Fig. 8. The difference between the 500 hPa average water vapor flux during August 14–17, 2016, and the climatological average water vapor flux during August 14–17 for the period 1980–2020 (a). (units: g/(cm*s*hPa)). The vectors represent the direction of the water vapor flux. The right panel shows the clustering of backward water vapor trajectories (b).

lower atmosphere. The aerosol-heated air rises along the Himalayas, inducing local deep convection on the windward slope. Additionally, the release of latent heat from increased condensation at higher altitudes further contributes to the warming of the mid-to-upper levels.

The difference between the 500 hPa water vapor flux during the response event and the climatology is shown in Fig. 8a. There are two main moisture transport pathways guided by anomalous southwest winds. One pathway involves southwest winds transporting moisture from the Arabian Sea across the Pamir Plateau to the southwestern edge of the Tarim Basin in Xinjiang, China. The other pathway involves moisture carried by the Bengal cyclone from the Bay of Bengal. An anomalous anticyclone is present at 500 hPa, and the southeastern winds on its western side further strengthen the southeastern winds in the northeastern part of the Bengal cyclone, facilitating abundant moisture transport to the NWC compared to the previous pathway.

To further verify the moisture transport pathways mentioned above, backward trajectory analysis was conducted using the HYSPLIT4 model. The starting point for the analysis was selected at a location in the southeastern part of Xinjiang (36°N, 86°E), corresponding to the area with high precipitation. Since the southern edge of the Tarim Basin is at a higher elevation, with meteorological stations mostly located above 1300 m, and the moisture pathway of interest is at 500 hPa, the starting altitude for the simulations was set at 5000 m above ground level. The HYSPLIT4 model was used to track the backward trajectories starting from the initial point for 200 h and then retrack every 6 h for another 200 h. Multiple moisture trajectories were obtained and subjected to cluster analysis. The clustering results of the backward moisture trajectories are shown in Fig. 8b. In this extreme precipitation event, the moisture in the southeastern part of NWC mostly originated from the Bay of Bengal.

The predominant moisture transport influencing the precipitation during this event is characterized by meridional (north-south) flow. In the vertical profile of moisture flux (Fig. 9a), a significant accumulation of moisture is observed in the lower troposphere along the southern slope of the Tibetan Plateau. This region is characterized by an anomalous center of high temperatures (Fig. S3c) and upward motion, indicating a strengthened ascent of moist air in the lower and middle troposphere. The terrain plays a crucial role, enhancing the "lift and cross" mechanism. Furthermore, anomalous southerly winds prevail in the middle and upper troposphere, facilitating the northward transport of moisture. The shaded area represents the terrain, and a small amount of moisture is transported by these anomalous southerly winds into the interior of the plateau and the arid regions of NWC.

Although the moisture flux in the middle and upper troposphere is relatively modest, its contribution is of great importance to the arid regions of northwest China, where annual precipitation is typically only a few tens of millimeters. Thus, while the lower troposphere predominantly facilitates moisture transport, the moisture flux in the middle and upper troposphere significantly impacts the water resources in the arid regions.

The vertical integration of meridional moisture flux highlights the primary high-value center along the southern slope of the Tibetan Plateau. Due to the obstruction of the high terrain, the majority of moisture is unable to cross the plateau and reach the arid regions. However, the edge of the Tarim Basin and the northern part of Gansu province exhibit positive anomalies in meridional moisture flux, indicating abnormal meridional moisture transport in these areas. The formation of an extreme precipitation event usually takes several days. Analyzing the temporal variation of moisture flux magnitude is crucial. The Fig. 9b reflects the gradual northward movement of the anomalous high-value center of moisture flux from August 15th to 17th, encompassing the entire period.

In the analysis of meteorological fields during this response event (Key Response Area I), a prominent anomaly is observed in the
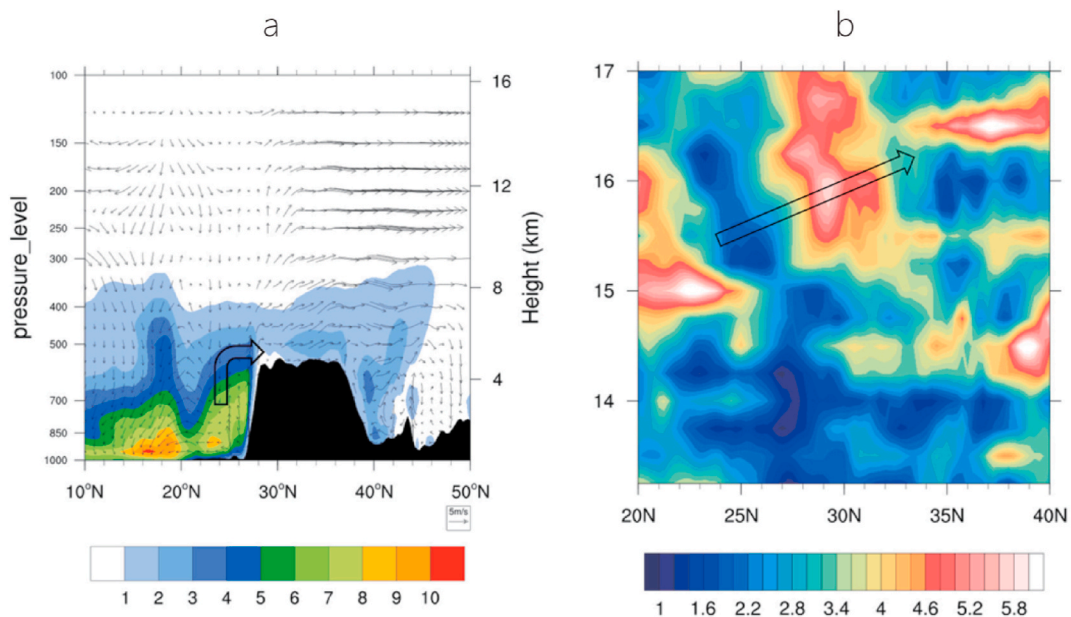
Fig. 9. Composite profile of anomalous water vapor flux overlaid with vertical and meridional wind anomalies (a); Time-latitude profile of anomalous water vapor flux magnitude (b) (units: g/cm*s*hPa), averaged over 85°E to 92°E.

lower atmosphere's temperature field over the southern slope of the Tibetan Plateau. Due to abnormal heating, influenced by the terrain, the atmosphere on the southern side of the Himalayas begins to ascend. Additionally, the enhanced Bengal cyclone and the anomalous anticyclone work in conjunction, strengthening the southerly winds. As a result, the uplifted warm and moist air traverses the Tibetan Plateau and is transported to the arid southern Xinjiang region. This phenomenon is likely one of the significant contributing factors to the formation of this extreme precipitation event.

3.2.2. Case study in the Key Response Zone II

The synthesis of five extreme precipitation events that occurred in the Qinghai is conducted. The five events occurred on August 21, 1993, July 12, 2002, June 16, 2007, August 25, 2008, and June 15, 2011. The daily average precipitation for these extreme events is shown in Fig. S4. The high precipitation values are mainly concentrated in the southwest of Qinghai, with two precipitation centers located at the junction of Qinghai and Gansu provinces in the Qilian Mountains. The daily average precipitation for these five extreme events can reach up to 9 mm/day, as compared to the 90th percentile precipitation threshold shown in Fig. 6b for the climatology average.

During the synthesis of meteorological fields for the five extreme precipitation events in Qinghai, it was observed that the Gangetic Plain in South Asia exhibited high values of AOD (Fig. 10a). The AOD values were more than 60 % compared to the climatological average, indicating a pollution event in this region. The high AOD values were primarily concentrated in the northern part of South Asia, where the South Asian summer monsoon transported aerosols northward over India. The presence of high mountains like the Himalayas acted as a barrier, causing the aerosols to concentrate mainly in the northern part of India during the summer season.

The AOD of black carbon, dust, organic carbon, sea salt, and sulfate aerosols were calculated and compared to their climatological values within the South Asia regional average (20°-30°N, 66.5°-100°E) (Fig. 10b). Dust aerosols exhibited a significant positive anomaly compared to the climatological average, particularly during the case 2 event, where the dust AOD was nearly 140 % greater than the climatological average. Black carbon and organic carbon aerosols also showed elevated levels during the five response events, indicating high emissions of these aerosols.

Using radiation data from ERA5 in clear sky conditions, the atmospheric top net downward shortwave radiation is subtracted from the surface net downward shortwave radiation to obtain the column-integrated atmospheric absorption of shortwave radiation. The difference between the column-integrated atmospheric absorption of shortwave radiation during the response event and the 1980–2020 summer climatology is calculated (Fig. 11a). During the response event, the South Asian continent absorbs more shortwave radiation in the atmospheric column compared to the climatology, which may be due to an abnormal increase in absorbing aerosols such as dust aerosols, black carbon, and other absorbing aerosols.

Due to the "elevated heating pump" effect of South Asian aerosols, there may be localized heating of the atmosphere in the northern parts of South Asia due to an abnormal increase in dust aerosols and black carbon aerosols. This leads to the ascent of warm and moist air along the Himalayas. The anomalous heating in South Asia, the Bay of Bengal, and the Tibetan Plateau can alter local circulation patterns and potentially cause changes in large-scale circulation, including the South Asian summer monsoon. The vertical variation of the temperature field (Fig. 11b) reflects the presence of an abnormal high-value center on the southern side of high mountain ranges, which, combined with the topographic lifting effect, can lead to localized deep convection.

To facilitate precipitation, it is necessary to have favorable moisture conditions and the interaction of convective motions. In Qinghai, the primary moisture pathway is the northern moisture channel, which involves the transport of moisture from the Black Sea and the Caspian Sea towards the southeast. Another moisture pathway involves the convergence of moisture from the Bay of Bengal and the westerly jet stream, which is then transported northwards to the Qinghai by the South Asian summer monsoon.

Typically, due to the obstruction of the Tibetan Plateau, the moisture transport to the plateau is relatively weak. However, analyzing the anomalous moisture transport during the response event (Fig. 12), it is observed that there is an anomalous southerly wind at 700 hPa (Fig. 12a), which transports moisture from the Bay of Bengal to the southern edge of the Tibetan Plateau. As a result, moisture accumulates in this region. The southwestern wind at 500 hPa continues to transport moisture to Qinghai, with moisture from the Bay of Bengal relayed to Qinghai by the low-level southerly wind in the troposphere. The anomalous divergence of the integrated moisture flux (Fig. 12b) reflects the anomalous moisture convergence in Qinghai, which is closely related to the formation of extreme precipitation events.

The anomalous increase in aerosols in the northern part of South Asia plays a significant role in the five extreme precipitation events observed in Qinghai. The increased aerosols, particularly in the southern slopes of the Tibetan Plateau and the northwest of the South Asian subcontinent, lead to positive temperature anomalies in the local lower to middle atmosphere. These anomalies trigger the occurrence of deep convection in the region. Under the influence of the South Asian aerosol-induced elevated heating pump effect, which can enhance the South Asian monsoon. This, in turn, increases the moisture transport from the eastern side of the plateau to Qinghai, leading to the occurrence or intensification of extreme precipitation events.

4. Summary and discussion

This study analyzes the spatiotemporal characteristics of AOD in South Asia and extreme precipitation events in the NWC from 1980 to 2020 using CN05.1 daily precipitation data, ERA5, and MERRA-2 reanalysis data. Different statistical methods and time scales are used to analyze the correlation between AOD in South Asia and precipitation in the NWC. Two key aerosol-precipitation response regions are identified: the southern Xinjiang and Qinghai. The meteorological fields of these regions during the response events are synthesized to explore their potential impact mechanisms. The main conclusions of this study are as follows:

The seasonal mean AOD in South Asia shows significant fluctuations and interannual variations from 1980 to 2020. During the pre-
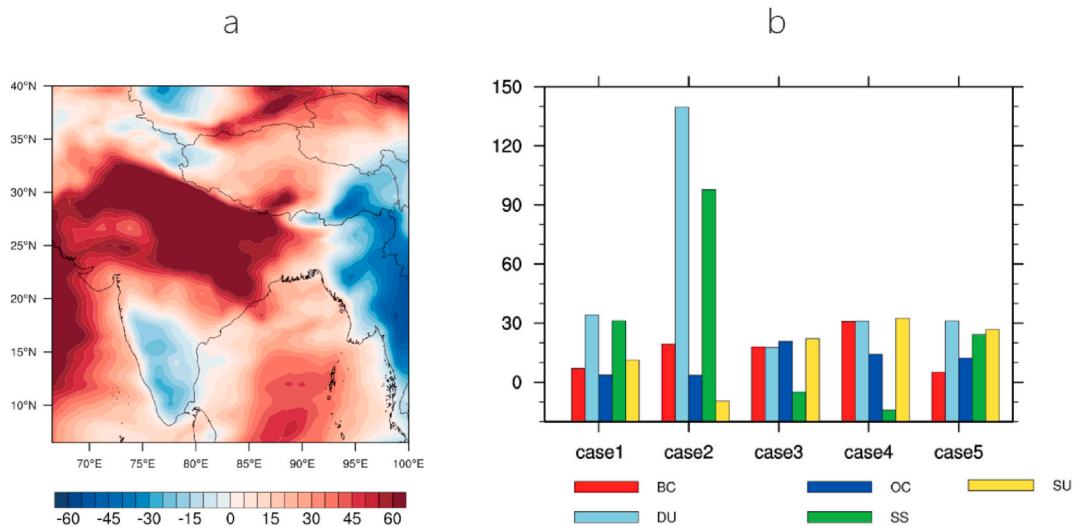
Fig. 10. The percentage departure from the 1980–2020 summer climatological average for the averaged AOD during extreme events in the South Asia region (a) (unit: %); Percentage departure from the 1980–2020 summer climatological average for black carbon, dust, organic carbon, sea salt, and sulfate AOD during the five response events (b) (unit: %).
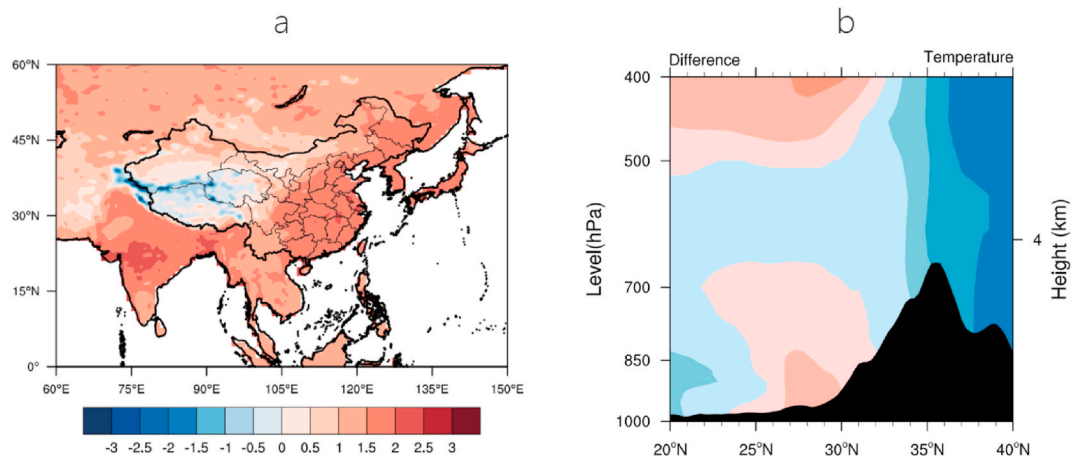

Fig. 11. a: the difference of the atmospheric net shortwave radiation between the synthesized response event (three days) and the 1980–2020 summer average (unit: kw*h/m²). b: A cross-sectional plot (unit: K) of the difference of the temperature between synthesized the response event (three days) and the 1980–2020 summer average, averaged over 65°E to 80°E.

monsoon season, there is a significant increase in AOD, while during the monsoon season, the increasing trend is smaller. The spatial distribution of the AOD trend in South Asia varies, but the regions with the largest increase in seasonal mean AOD are generally concentrated in the northern part of the Indian subcontinent.

The extreme precipitation indices in the NWC, except for CDD, show an increasing trend. The indices R95PTOT, R99PTOT, PRCPTOT, and R10 exhibit similar spatial distributions, with strong increasing trends in the Tianshan Mountains, Qilian Mountains, and eastern Qinghai Province. There is a correlation between AOD in South Asia and extreme precipitation indices in the NWC. In particular, some extreme precipitation indices in the southern Tarim Basin of southern Xinjiang, Qinghai, and northern Gansu have correlation coefficients more than 0.4 with the AOD time series in South Asia.

There are two key response regions for aerosols and extreme precipitation: the southern Xinjiang and Qinghai. These regions exhibit strong positive correlations between AOD in South Asia and extreme precipitation in the NWC. During extreme precipitation events in these regions, the AOD in South Asia is generally elevated, indicating a simultaneous occurrence of heavy aerosols and extreme precipitation events in the NWC.

In the synthetic analysis of a response event in the southern Xinjiang, there is an anomalous high AOD zone in the northern part of South Asia. The increased absorption aerosols result in an anomalous heating layer in the lower to middle atmosphere of the southern slopes of the Tibetan Plateau, which strengthens the "lift and cross" mechanism of moisture transport along the mountains. The
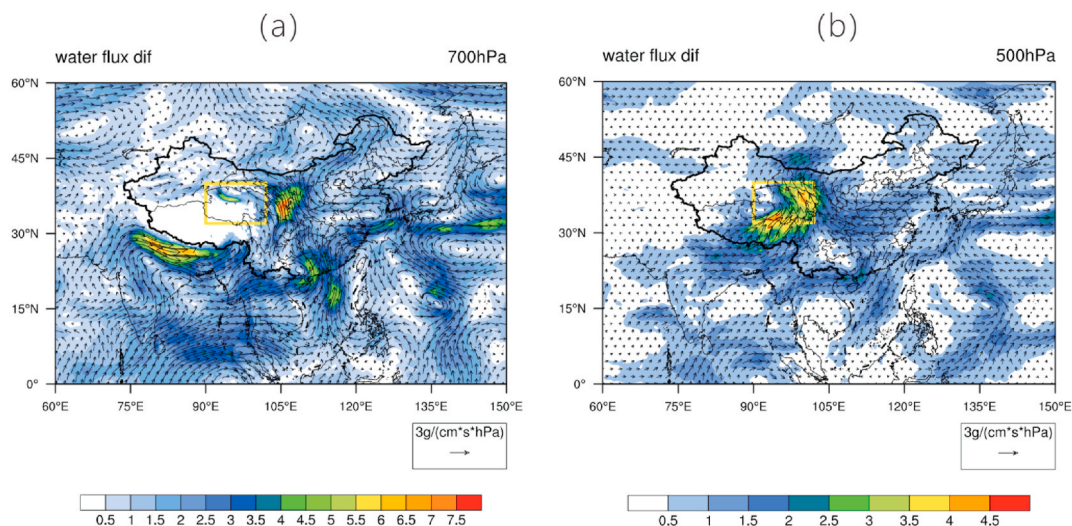
Fig. 12. The difference between synthesized response events and the 1980–2020 summer average of specific humidity flux at 700 hPa (a) and 500 hPa (b). The vector arrows represent the direction of specific humidity flux, and the color shading indicates the magnitude of specific humidity flux in units of g/(cm*s*hPa). The yellow box represents the study area. (For interpretation of the references to color in this figure legend, the reader is referred to the Web version of this article.)

enhanced South Asian monsoon and the interaction between the anomalous strengthened monsoon and anticyclone lead to enhanced southerly winds, which transport moisture over the Tibetan Plateau to the arid southern Xinjiang, triggering extreme precipitation.

In the synthetic analysis of five response events in Qinghai, the AOD in South Asia is more than 60 % higher than the climatology, with significant contributions from absorbing aerosols such as black carbon and dust aerosols. The direct radiative effect of aerosols results in anomalous heating in the lower to middle atmosphere of South Asia, with high-temperature anomalies mainly located in the northern part of the South Asian subcontinent and the Bay of Bengal. The anomalous atmospheric heating triggers local convection in the northern part of the South Asian subcontinent, and under the South Asian aerosol-induced elevated heating pump effect, the Tibetan Plateau experiences an anomalous high-temperature center. This strengthens the South Asian summer monsoon, and the anomalous southwestern airflow brings warm and moist air around the eastern side of the Tibetan Plateau, leading to extreme precipitation events in Qinghai Province.

It is important to recognize that the formation of precipitation is a complex process influenced by multiple factors. It cannot be simplistically attributed to a single cause. Even in the localized formation of precipitation, aerosols do not have a decisive role. The Northwestern China experiences a dry climate with limited precipitation, resulting in a scarcity of statistical data and unfavorable statistical conditions. Due to these factors, there are inherent challenges in explaining the mechanisms, and this study only establishes a certain connection between the two factors using climate statistical methods, with some limitations in mechanistic interpretation. Climate models have been extensively employed, particularly in studying the climate effects of aerosols. However, the reanalysis data used in this study is unable to isolate the influence of aerosols on climate, lacking the validation provided by models—an essential tool. Conducting sensitivity experiments using atmospheric chemistry models, specifically by altering aerosols as a single variable to observe the corresponding precipitation response, would be an ideal approach. Nevertheless, given the lower accuracy of precipitation simulation in regions such as the Tibetan Plateau, it is expected that model simulations will encounter challenges. Consequently, there is ample scope for future improvements in this regard, including the utilization of atmospheric chemistry models for sensitivity experiments and addressing the difficulties associated with accurate precipitation simulation in regions like the Tibetan Plateau.

Data availability statement

The authors do not have permission to share data. The reanalysis data used in the article can be registered and downloaded through public web pages.

CRediT authorship contribution statement

Zhenming Ji: Writing – review & editing, Writing – original draft, Validation, Supervision, Resources, Methodology, Investigation, Formal analysis, Data curation, Conceptualization. **Shuting Tian:** Validation, Supervision, Software, Methodology.

Declaration of competing interest

The authors declared that they have no conflicts of interest in connection with the manuscript submitted.

Acknowledgments

Appendix A. Supplementary data

Supplementary data to this article can be found online at https://doi.org/10.1016/j.heliyon.2024.e30826.

References

[1] Y. Shi, Y. Shen, D. Li, G. Zhang, Y. Ding, R. Hu, et al., Discussion on the present climate change from warm-dry to warm wet in northwest China, Quat. Sci. 23 (2) (2003) 152–164.
[2] Y. Shi, Y. Shen, E. Kang, D. Li, Y. Ding, G. Zhang, et al., Recent and future climate change in northwest China, Climatic Change 80 (2007) 379–393.
[3] C. Wang, S. Zhang, F. Zhang, K. Li, K. Yang, On the increase of precipitation in the Northwestern China under the global warming, Adv. Earth Sci. 36 (2021) 980–989.
[4] R. Chen, Y. Shen, W. Mao, S. Zhang, H. Lv, Y. Liu, et al., Progress and issues on key technologies in forecasting of snowmelt flood disaster in arid areas Northwest China, Adv. Earth Sci. 36 (3) (2021) 233–244.
[5] X. Guan, L. Yang, Y. Zhang, J. Li, Spatial distribution, temporal variation, and transport characteristics of atmospheric water vapor over Central Asia and the arid region of China, Global Planet. Change 172 (2019) 159–178.
[6] S. Lu, Z. Hu, H. Yu, W. Fan, C. Fu, D. Wu, Changes of extreme precipitation and its associated mechanisms in Northwest China, Adv. Atmos. Sci. 38 (2021) 1665–1681.
[7] Q. Zhang, J. Yang, W. Wang, P. Ma, G. Lu, X. Liu, et al., Climatic warming and humidification in the arid region of Northwest China: multi-scale characteristics and impacts on ecological vegetation, Journal of Meteorological Research 35 (1) (2021) 113–127.
[8] M. Guo, Z. Wang, A. Qin, Y. Fan, Changes in precipitation in Northwest China over the last 54 years, Arid Zone Res. 26 (2009) 120–125.
[9] F. Chen, J. Chen, W. Huang, Weakened East Asian summer monsoon triggers increased precipitation in Northwest China, Sci. China Earth Sci. 64 (5) (2021) 835–837.
[10] W. Huang, S. Feng, J. Chen, F. Chen, Physical mechanisms of summer precipitation variations in the Tarim Basin in northwestern China, J. Clim. 28 (9) (2015) 3579–3591.
[11] W. Huang, S.-Q. Chang, C.-L. Xie, Z.-P. Zhang, Moisture sources of extreme summer precipitation events in North Xinjiang and their relationship with atmospheric circulation, Adv. Clim. Change Res. 8 (1) (2017) 12–17.
[12] K. Lau, M. Kim, K. Kim, Asian summer monsoon anomalies induced by aerosol direct forcing: the role of the Tibetan Plateau, Clim. Dynam. 26 (2006) 855–864.
[13] S. Nigam, M. Bollasina, "Elevated heat pump" hypothesis for the aerosol-monsoon hydroclimate link, "Grounded" in observations? Journal of Geophysical Research: Atmosphere 115 (D16) (2010).
[14] M. Wonsick, R. Pinker, Y. Ma, Investigation of the" elevated heat pump" hypothesis of the Asian monsoon using satellite observations, Atmos. Chem. Phys. 14 (16) (2014) 8749–8761.
[15] M. D`Errico, C. Cagnazzo, P.G. Fogli, W.K. Lau, J. von Hardenberg, F. Fierli, et al., Indian monsoon and the elevated-heat-pump mechanism in a coupled aerosol-climate model, J. Geophys. Res. Atmos. 120 (17) (2015) 8712–8723.
[16] C.E. Chung, V. Ramanathan, Weakening of North Indian SST gradients and the monsoon rainfall in India and the Sahel, J. Clim. 19 (10) (2006) 2036–2045.
[17] Z. Wang, H. Zhang, P-w Guo, Effects of black carbon aerosol in South Asia on Asian summer monsoon, Plateau Meteorol. 28 (2) (2009) 419–424.
[18] Z. Ji, S. Kang, D. Zhang, C. Zhu, J. Wu, Y. Xu, Simulation of the anthropogenic aerosols over South Asia and their effects on Indian summer monsoon, Clim. Dynam. 36 (2011) 1633–1647.
[19] D. Singh, M. Bollasina, M. Ting, N.S. Diffenbaugh, Disentangling the influence of local and remote anthropogenic aerosols on South Asian monsoon daily rainfall characteristics, Clim. Dynam. 52 (2019) 6301–6320.
[20] D.M. Westervelt, Y. You, X. Li, M. Ting, D.E. Lee, Y. Ming, Relative importance of greenhouse gases, sulfate, organic carbon, and black carbon aerosol for South Asian monsoon rainfall changes, Geophys. Res. Lett. 47 (13) (2020) e2020GL088363.
[21] Z. Li, W.M. Lau, V. Ramanathan, G. Wu, Y. Ding, M. Manoj, et al., Aerosol and monsoon climate interactions over Asia, Rev. Geophys. 54 (4) (2016) 866–929.
[22] W. Du, S. Kang, X. Qin, Z. Ji, W. Sun, J. Chen, et al., Can summer monsoon moisture invade the Jade Pass in Northwestern China? Clim. Dynam. 55 (2020) 3101–3115.
[23] D. Ayantika, R. Krishnan, M. Singh, P. Swapna, N. Sandeep, A. Prajeesh, et al., Understanding the combined effects of global warming and anthropogenic aerosol forcing on the South Asian monsoon, Clim. Dynam. 56 (2021) 1643–1662.
[24] G. Ning, M. Luo, Q. Zhang, S. Wang, Z. Liu, Y. Yang, et al., Understanding the mechanisms of summer extreme precipitation events in Xinjiang of arid Northwest China, J. Geophys. Res. Atmos. 126 (15) (2021) e2020JD034111.
[25] J. Wu, X.-J. Gao, A gridded daily observation dataset over China region and comparison with the other datasets, Chin. J. Geophys. 56 (4) (2013) 1102–1111.
[26] C. Randles, A. Da Silva, V. Buchard, P. Colarco, A. Darmenov, R. Govindaraju, et al., The MERRA-2 aerosol reanalysis, 1980 onward. Part I: System description and data assimilation evaluation, J. Clim. 30 (17) (2017) 6823–6850.
[27] L. He, X. Hao, H. Li, T. Han, How do extreme summer precipitation events over eastern China subregions change? Geophys. Res. Lett. 48 (5) (2021) e2020GL091849.
[28] Y. Tang, A. Huang, P. Wu, D. Huang, D. Xue, Y. Wu, Drivers of summer extreme precipitation events over East China, Geophys. Res. Lett. 48 (11) (2021) e2021GL093670.